Hindawi Publishing Corporation
Journal of Nanomaterials
Volume 2014, Article ID 284612, 13 pages
http://dx.doi.org/10.1155/2014/284612

Research Article

Interlamellar Space Configuration under Variable Environmental Conditions in the Case of Ni-Exchanged Montmorillonite: Quantitative XRD Analysis

Marwa Ammar,[1] Walid Oueslati,[1,2] Nejmeddine Chorfi,[3] and Hafsia Ben Rhaiem[1]

[1] *UR05/13-01, Physique des Matériaux Lamellaires et Nano-Matériaux Hybrides (PMLNMH), Faculté des Sciences de Bizerte, 7021 Zarzouna, Tunisia*
[2] *General Studies Department, College of Electronics & Communications, Technical and Vocational Training Corporation, TV Street, P.O. Box 2816, Jeddah 21461, Saudi Arabia*
[3] *Department of Mathematics, College of Science, King Saud University, P.O. Box 2455, Riyadh 11451, Saudi Arabia*

Correspondence should be addressed to Walid Oueslati; walidoueslati@ymail.com

Received 11 August 2014; Revised 27 October 2014; Accepted 30 October 2014; Published 27 November 2014

Academic Editor: Edward A. Payzant

Interlamellar space organization of low-charge montmorillonite was studied by modeling of X-ray diffraction (XRD) patterns recorded under controlled relative humidity (RH) conditions on Ni saturated specimens. The quantitative XRD investigation, based on an indirect method consisting of the comparison of experimental 00ℓ reflections with the other calculated from structural models, is used to characterize eventual nanostructural changes along c^* axis of Ni-exchanged montmorillonite. This method allowed us to determine, respectively, the relative layer types contribution, the layer thickness, nanoconfiguration of the interlamellar space, and position, amount, and organization of water molecules and exchangeable cations. Obtained theoretical models exhibit heterogeneous hydration state which is the dominating character detected all over studied cycles. Along RH cycle a modification in the main structure of the host materials is performed and the presence of a mixed layer structure (MLS) is noted. The hydration hysteresis at the low and the high RH range can be explained by fluctuations in the water retention mechanism and hydration heterogeneities created within the smectite crystallite.

1. Introduction

The use of natural materials like clay minerals as a geological barrier to immobilize the metal cations, occurring essentially from industrial waste and household trash, presents one of the most economical solutions seen by their low cost and their ubiquitous presence in most soils [1–6]. In fact, smectites are a clay mineral, more precisely, a 2 : 1 type of aluminosilicate characterized by a high cation retention ability and low permeability and swelling. These properties make montmorillonite a material widely used as an engineered barrier in the context of waste disposal sites and suitable as sorbent material to remove the heavy metals principally stirring by ion-exchange mechanism. As clay minerals react quickly to changing environmental conditions [7], an accurate determination of the nature and composition of clay minerals is of high importance to assess their actual and short- and long-term impacts on the functioning of soil environments. However, such a precise identification of clay mineralogy is extremely complex because of their heterogeneity in clay mineral chemistry and structure at the sample, crystal, and layer scales. Indeed, several layer types commonly coexist within a wide range of particle sizes (from ~50 nm to ~5 μm) but can also be observed as mixed-layer phases in which different types of clay layers coexist in the same crystal [8]. Such a complex mineralogy can, however, be partially revealed and quantified by comparing experimental X-ray diffraction (XRD) patterns with profiles calculated by assuming discrete clay phases or mixed-layer structure (MLS). Based on the examination of 00ℓ basal reflections, a lot of studies have been done on the hydration properties of this clay in order to understand the interlamellar

space organization as function of relative humidity (RH) condition [9–16]. On the other hand, the interlayer water organization in presence of exchangeable heavy metal cations (i.e., Ni^{2+}) initiates the necessity to monitor the behavior of this barrier according to several climate changes and environmental factors that may affect the clay matrix in order to predict its short- and long-term performance. All earlier works report the importance and the performance of clay minerals especially montmorillonite to retain Ni(II) [17–27] ions. In the present study, an investigation of the effect of the relative humidity variations on the hydration performance of a Ni-exchanged montmorillonite is achieved. Indeed, this goal is accomplished during two humidifying/drying cycles. All structural material properties changes are monitored by quantitative XRD analysis using an indirect method based on the comparison between experimental 00ℓ reflections, obtained "*in situ*" under controlled atmosphere, and theoretical ones.

2. Materials and Methods

2.1. Starting Sample. A reference dioctahedral smectite SWy-2 originated from bentonites of Wyoming (Wyoming, USA) is selected for the present study. Clay fraction is supplied by the Source Clay Minerals Repository Collection of The Clay Minerals Society (USA) [28, 29], exhibiting a low octahedral charge and extremely limited tetrahedral substitutions and presenting 101 meq/100 g as a Cation Exchange Capacity (CEC) [29]. Its half-cell structural formula, that is determined by [30], is as the following:

$$Si_{3.923}Al_{0.077}(Al_{1.459}Ti^{4+}_{0.018}Fe^{3+}_{0.039}Fe^{2+}_{0.045}Mg^{2+}_{0.382})O_{10}(OH)_2(Ca^{2+}_{0.177}Na^{+}_{0.027})$$

2.2. Pretreatment. A pretreatment with NaCl solution consists of guaranteeing total saturation of all exchangeable site, according to a classical protocol detailed by Tessier [31]. At first time an Na^+ exchange process is performed in order to prepare an Na-rich montmorillonite suspension labeled SWy-2-Na. The XRD analysis is used to characterize this process. A simple comparison between original and treated sample is reported in Figure 1.

At second time, the CEC of the obtained SWy-2-Na fraction is saturated with the divalent cations Ni^{2+} and the obtained suspension is referred to as SWy-2-Ni. The ionic exchange process is conducted using the following protocol summarized in Figure 2. Oriented preparations, for the XRD analysis, are obtained by depositing SWy-2-Ni suspension onto a glass slide and drying it at room temperature for 24 hours to acquire an air-dried specimen [32].

2.3. Experimental Procedure. All experimental XRD patterns are performed by reflection setting with a D8 Advance Bruker installation using Cu-Kα radiation equipped with solid-state detector and operating at 40 KV and 30 Ma. The diffractometer was equipped with an Ansyco rh-plus 2250 humidity control device coupled to an Anton Paar TTK450 chamber. The XRD patterns are registered every 10% RH scale at the fixed relative humidity conditions values. The usual scanning parameters were 0.04 $2\theta^\circ$ as step size and 6 s as counting time per step over the angular range 2–40 $2\theta^\circ$. The divergence slit, the two Soller slits, the antiscatter, and receiving slits were 0.5, 2.3, 2.3, 0.5, and 0.06°, respectively.

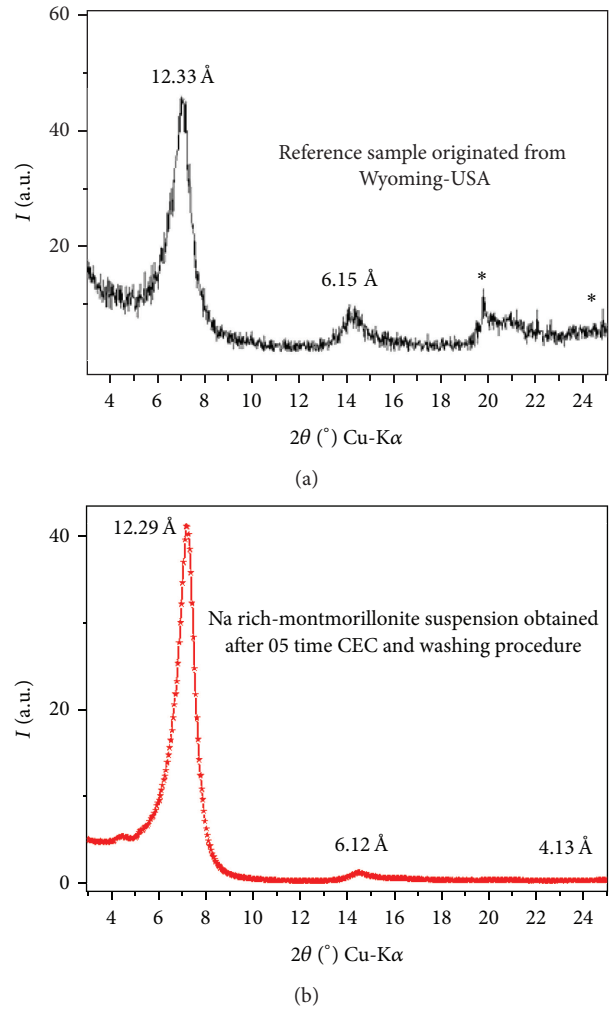

Figure 1: Experimental XRD patterns of original (a) and treated SWy sample (b) with NaCl solution.

2.4. Relative Humidity Sequence Orientation. To carry out the first humidifying cycle, the RH value extends from 40%, the room condition (297 K and ~40% RH), to the almost saturated condition (80% RH). In second time, a dehydration procedure is realized by decreasing the RH rates to extremely dry ones (10% RH), and finally a second return to 40% RH is adopted. The reverse cycle is accomplished by varying the moisture values in the opposite direction starting the dehydration process from 40% RH and decreasing toward extremely dry ones (10% RH) followed by a continuous RH increase towards 80%. The end of the cycle is done by a second dehydration procedure by decreasing again the relative humidity rates to 40% RH. These cycles will be referred to, respectively, as the hydration/dehydration and

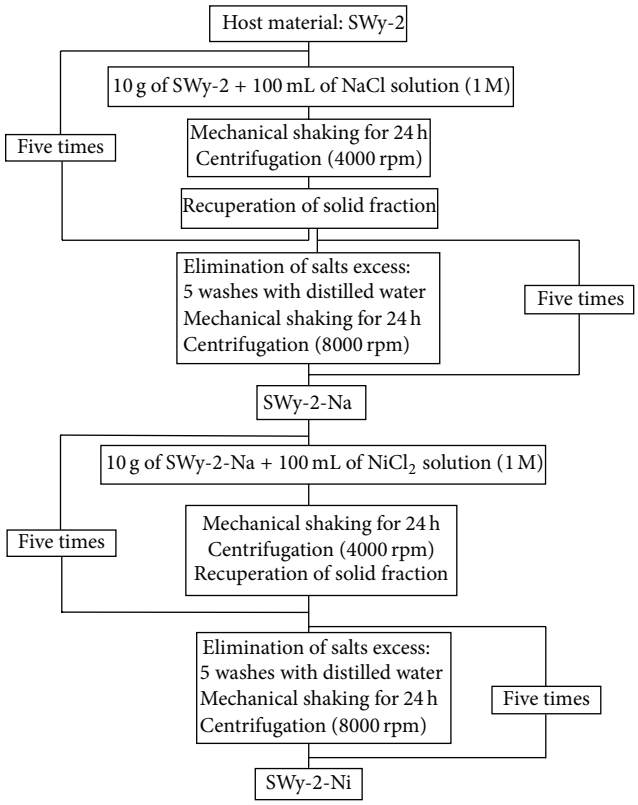

Figure 2: Experimental ionic exchange process.

the dehydration/hydration, for the first and the second RH variation sequence. The sequence orientation of %RH rates in both cycles is described in detail in Figure 3.

2.5. The Moisture Equilibration. An object reaches moisture equilibrium with the environment when it neither gains nor loses moisture from the constant, dynamic exchange of moisture with the environment. The process of hygroscopic materials to reach equilibrium with the ambient relative humidity of the air, by absorbing or desorbing moisture, is controlled by XRD analysis. In Figure 4 the stability of the 001 reflection is controlled using XRD analysis.

2.6. X-Ray Diffraction

2.6.1. Interlamellar Water Molecules Organization. The X-ray diffraction (XRD) has been a powerful technique often used to study hydration proprieties. In fact, different layer types were defined for smectite as a function of the d_{001} spacing values: dehydrated (0W, d_{001}) (9.7–10.2 Å), monohydrated (1W, d_{001}) (11.6–12.9 Å), bihydrated (2W, d_{001}) (14.9–15.7 Å), and trihydrated (3W, d_{001}) (18-19 Å) layers, corresponding, respectively, to the intercalation of 0, 1, 2, or 3 planes of H_2O molecules in the interlamellar spaces [33]. In the case of "0W" state, the interlayer spaces are devoid of water and the compensating cations are located in the middle of the interlamellar space and, in some cases, partially engage in the ditrigonal cavity. For the monohydrated layer "1W," both exchangeable cations and H_2O molecules are located in the mid-plane of the interlamellar space. For the bihydrated layers "2W," the cation is surrounded on both sides by the water molecules. In the case of "3W" hydration state, the exchangeable cations are strongly hydrated, situated with a plane of water in the medium of the interlamellar space, and surrounded by two water layers on both sides of the median plane of interlayer space. Moreover, most often different hydration states/layer types usually coexist within the same crystals even under controlled conditions [34–36]. Thus, the use of the XRD profile modeling techniques allows the investigation of the structures in which different hydration states coexist and the interlayer water content at any stage of the studied cycles.

2.6.2. Qualitative XRD Patterns Investigations. The qualitative XRD study provides information concerning the hydration state of the studied sample at a different RH rate, which are obtained by the position of the 001 reflexion (d_{001} basal spacing values) and the global description of the profile geometry (peaks symmetry and/or asymmetry). Moreover, the calculation of the full width at half-maximum intensity (FWHM) value and the standard deviation of the departure from rationality (ξ) related to the 00ℓ reflection (calculated as the standard deviation of the $l \times d(00\ell)$ values for all X_i measurable reflections over the explored $2\theta^\circ$ angular range) can supply information about the hydration heterogeneities degree (homogenous or interstratified) [37]. However, the qualitative interpretation of the XRD profile cannot provide a detailed insight related to the relative proportions of layers with different hydration states, which can coexist in the structure, and is unable to follow the evolution of certain structural parameters, such as the position and organization of exchangeable cations with H_2O molecule in the interlamellar space along the c^* axis, as function of relative humidity along both cycles. Thus it is necessary to perform the quantitative analysis [38, 39].

2.6.3. Quantitative XRD Analysis. The quantitative analysis is achieved using the X-ray profile modeling method based on the algorithms developed by [40] which consist of adjusting the experimental patterns (00ℓ peak series) to theoretical ones calculated using the Z atomic coordinates of the interlayer space corresponding to those proposed by [41] and the interlamellar water molecule distribution in accordance with the literature's description [42]. The theoretical intensities were calculated according to the matrix formalism detailed by [40]. The fitting strategy of 001 reflections is described by [42]. This method allows the determination of the interlamellar hydrations amounts and structural characteristics along the normal to the (Z) plane, in particular the number and the position of the exchanged cations and water molecules, the stacking layer thicknesses, and the stacking mode along c^* axis. The abundances of the different types of layers (Wi), the mode of stacking of the different kinds of layers, and the mean number of layers per Coherent Scattering Domain (CSD) can be also determined through XRD profile modeling approach. Within a CSD, the stacking of layers is described by

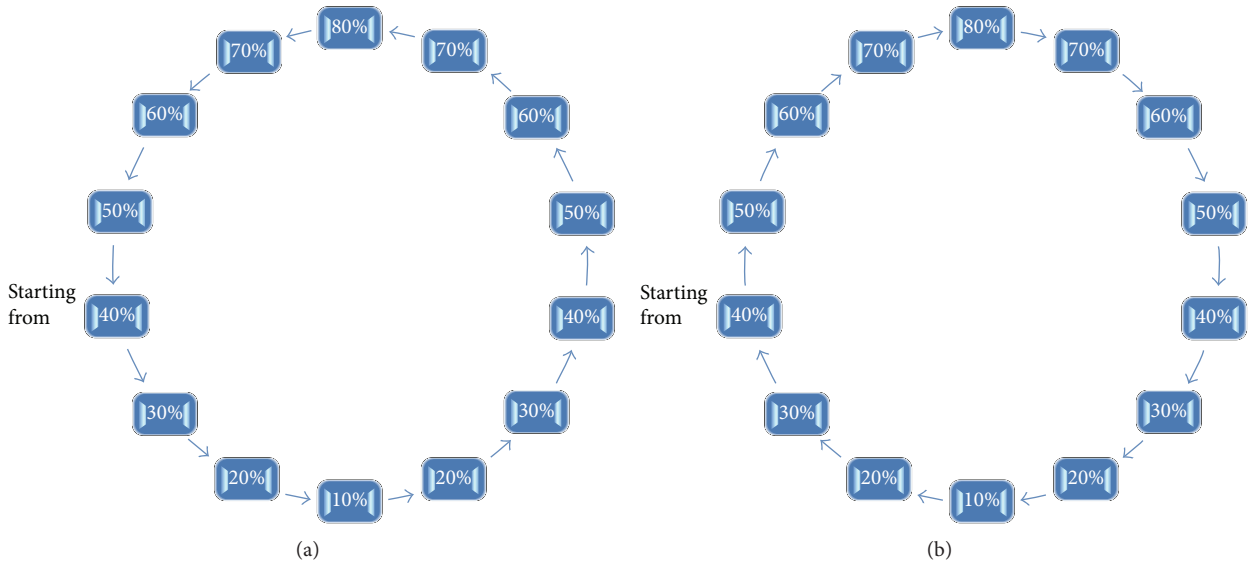

Figure 3: The sequence orientation of %RH rates along hydration/dehydration cycles.

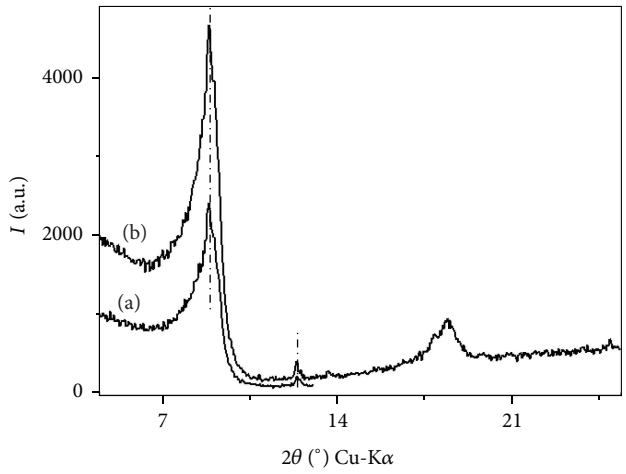

Figure 4: Stability of the 001 reflection is controlled using XRD analysis.

a set of junction probabilities (Pij). The relationships between these probabilities and the abundances Wi of the different types of layer are given by [41].

3. Results and Discussion

The best agreement between theoretical and experimental XRD patterns recorded under controlled RH condition, respectively, along the first and second cycles, is reported in Figures 5 and 6. All variable mixed-layer structures contributions (MLS) used to calculate experimental profiles are reported in the same figure. The results through the qualitative investigation, in regard, respectively, to the d_{001} basal spacing value, the FWHM of the 001 reflection, and the ξ parameter (i.e., which is calculated for 3 or 4 measurable reflections over the 2–40 2θ° angular range), were calculated for all experimental patterns and are summarized in Table 1 for both cycles. The composition of the MLSs and all structural parameters are reported in Tables 2 and 3, respectively, for the first and the second cycle.

3.1. Case of the Hydration-Dehydration Cycle

3.1.1. Qualitative XRD Description. The gradual progress of the d_{001} basal spacing value deduced from the 001 reflection positions showed that along the cycle two hystereses appear at two different RH domains that can be divided into two subcycles (Figure 7(a)).

The first one begins from 40% RH with a d_{001} 15.58 Å attributed to a homogeneous "2W hydration state," reaching 17.10 Å towards the extremely saturated conditions (i.e., 80% RH) then downing to return again at 40% RH with a d_{001} corresponding to a homogeneous "2W hydration state" (Table 1). Throughout this path, the studied sample presents a heterogeneous hydration behavior characterized by a continuous hydration transition between 2W and 3W expect at both 40% RH starting and downing. This continuous transition was accompanied by an increase in the FWHM value at the higher RH range indicating the interstratified hydration character (Table 1). The second subcycle spreads out over the lower RH range starting from the downing 40% RH and continues the dehydration process to the extremely dried condition (10% RH) where the d_{001} basal spacing shifts to 12.14 Å. This RH decrease is accompanied by a fast transition from 2W to 1W state which indicates the existence of heterogeneous hydration behavior over these %RH rates. The rehydration procedure performed by increasing the RH to return again at 40% RH is characterized by a slow 1W-2W transition and a slow d_{001} spacing values evolution (Table 1) that create a clear hysteresis buckle at the lower RH range (Figure 7(b)). Over this subcycle, an irrationality for all measurable reflection position was observed accompanied by

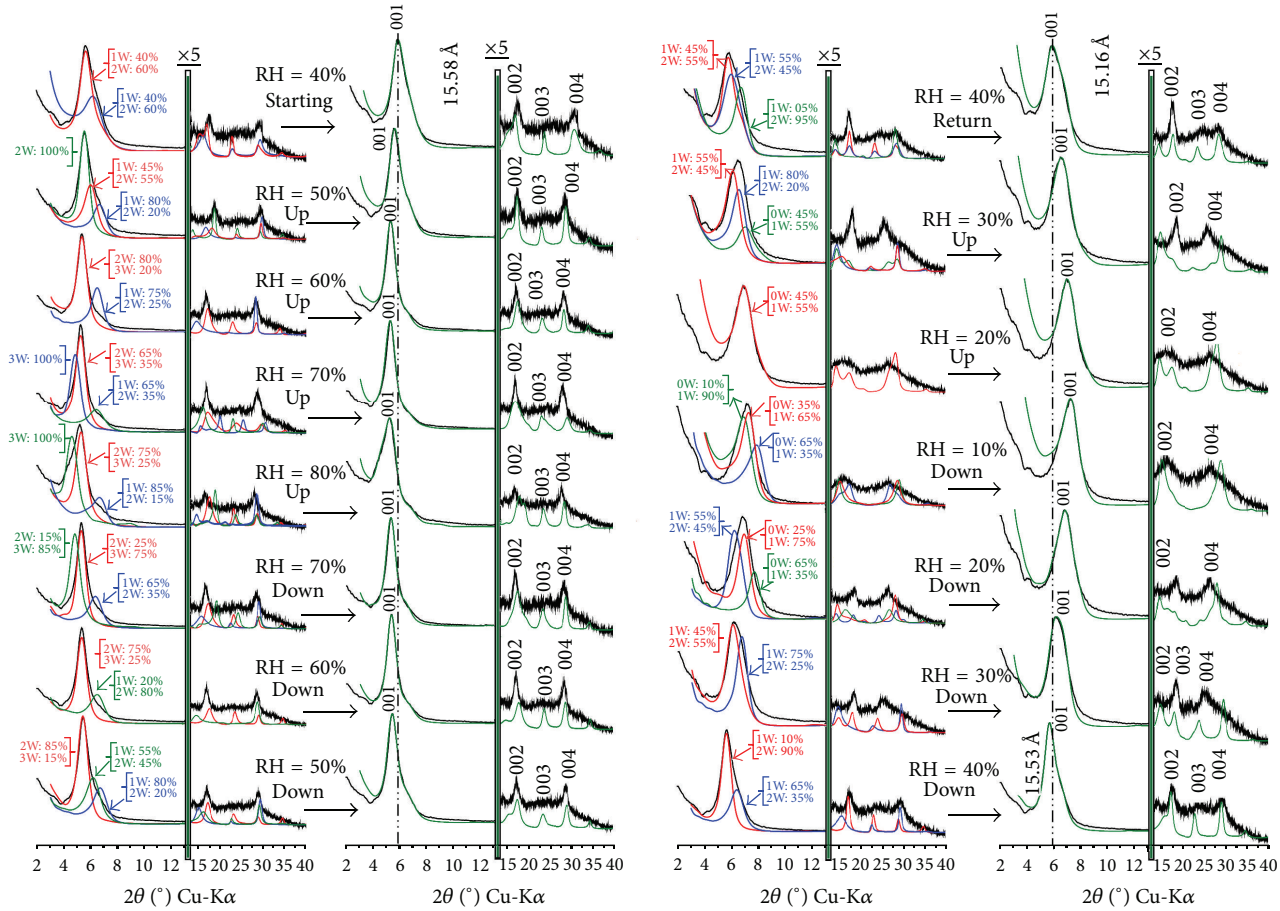

Figure 5: Different contributions of the various mixed-layer structures used to calculate XRD profiles in the case of the first cycle.

Table 1: Qualitative XRD investigations for SWy-2-Ni.

First cycle					Second cycle				
% RH	d_{001} (Å)	FWHM (2θ°)	ξ, X_i	Character	% RH	d_{001} (Å)	FWHM (2θ°)	ξ, X_i	Character
40 (start)	15.58	1.20	0.15, 3	I	40 (start)	15.47			I
50	15.87	0.98	0.18, 3	H	30	14.23	1.44	0.25, 3	I
60	16.59	0.80	0.40, 3	H	20	13.50	1.55	0.45, 3	I
70	16.68	0.78	0.46, 3	I	10	12.89	1.76	0.84, 3	I
80	17.10	1.06	0.32, 3	I	20	13.32	1.69	0.53, 3	I
70	16.53	0.79	0.41, 3	I	30	14.07	1.67	0.51, 3	I
60	16.44	0.80	0.37, 3	H	40	14.82	1.72	0.80, 3	I
50	16.16	0.87	0.31, 3	H	50	15.25	1.63	0.36, 3	I
40	15.53	1.01	0.30, 3	I	60	15.59	1.60	0.15, 3	I
30	14.18	1.42	0.70, 3	I	70	16.10	1.04	0.20, 3	I
20	12.96	1.39	0.72, 3	I	80	16.88	1.00	0.49, 3	I
10	12.14	1.44	0.78, 3	I	70	16.31	0.95	0.20, 3	H
20	12.64	1.41	0.54, 3	I	60	16.01	1.19	0.18, 3	I
30	13.38	1.37	0.47, 3	I	50	15.60	1.46	0.15, 3	I
40 (return)	15.16	1.48	0.20, 3	I	40 (return)	15.20	1.60	0.10, 3	I

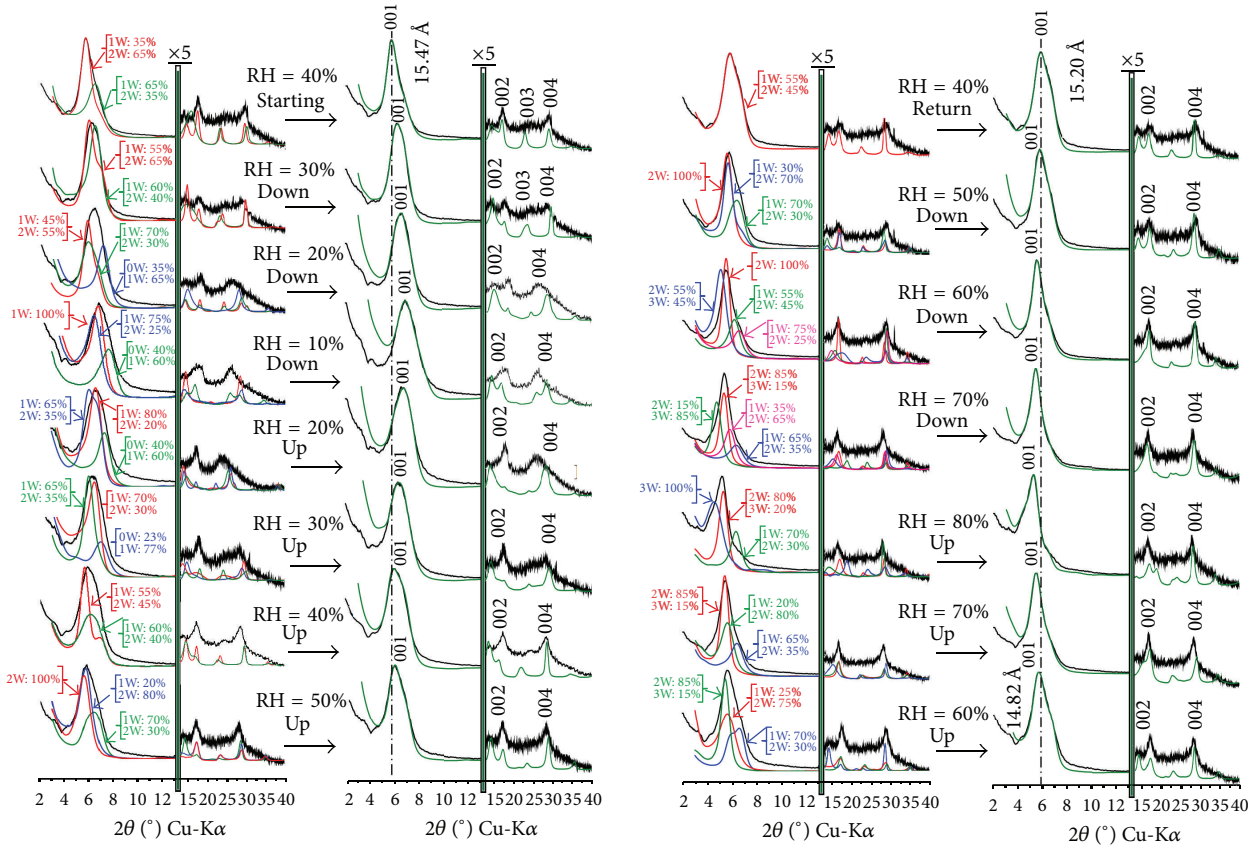

Figure 6: Different contributions of the various mixed-layer structures used to calculate XRD profiles in the case of the second cycle.

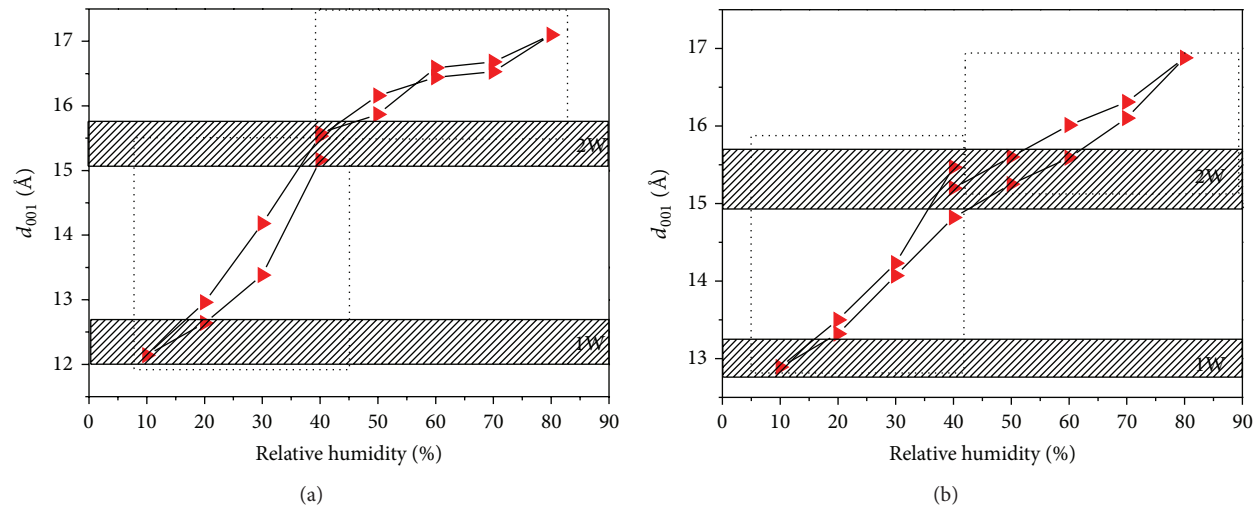

Figure 7: Pseudo hysteresis obtained, respectively, after hydration/dehydration (a) sequence and dehydration/hydration (b) sequence.

high ξ parameter values with an increase in the FWHM value (Table 1) signifying the heterogeneous hydration character.

3.1.2. Quantitative XRD Analysis

(1) Structure Heterogeneity Degree. The quantitative XRD investigation shows that all experimental profiles obtained over all RH range are fitted using structural models containing various MLSs (Figure 3). Thus the heterogeneous hydration character is systematically observed over the studied RH fields of this cycle. In fact at 40% RH, the proposed model is determined using two MLSs types characterized by interstratifications between 1W and 2W layer hydration state. The most hydration heterogeneity is detected at the

Table 2: Structural parameters used to reproduce experimental patterns of SWy-2-Ni as a function of RH along the first cycle.

	% RH	Layer type	L. Thck	n_{H_2O}	Z_{H_2O}	n_{Ni}	Z_{Ni}	Total contribution 0W/1W/2W/3W	M
Hydration procedure	40 (start)	0W	—	—	—	—	—	0/46.4/53.6/0	8
		1W	12.00	1.5	10.50	0.15	10.50		
		2W	15.75	3.6	11.30/14.50	0.15	12.80		
		3W	—	—	—	—	—		
	50	0W	—	—	—	—	—	0/36.60/63.40/0	9
		1W	12.30	1.7	10.00	0.15	10.00		
		2W	15.75	3.8	11.30/14.50	0.15	12.80		
		3W	—	—	—	—	—		
	60	0W	—	—	—	—	—	0/13.50/70.10/16.40	9
		1W	12.65	1.7	10.20	0.15	10.20		
		2W	15.85	4.2	11.00/14.00	0.15	12.80		
		3W	18.60	5.4	10.00/14.50/16.20	0.15	14.50		
	70	0W	—	—	—	—	—	0/17.47/54.33/28.20	8
		1W	12.00	2	10.50	0.15	10.50		
		2W	15.80	4.8	10.70/14.60	0.15	12.60		
		3W	18	6	10.20/14.70/16.50	0.15	14.70		
	80	0W	—	—	—	—	—	0/13.30/41.34/45.36	8
		1W	12.80	1.8	10.00	0.15	10.00		
		2W	15.85	5	11.00/13.50	0.15	12.40		
		3W	18.70	6.6	10.30/14.30/16.30	0.15	14.30		
Dehydration process	70	0W	—	—	—	—	—	0/19.34/58.90/4.41	8
		1W	12.30	2	10.00	0.15	10.00		
		2W	15.80	4.4	10.90/14.70	0.15	12.70		
		3W	18.50	6.6	10.50/14.90/16.20	0.15	14.90		
	60	0W	—	—	—	—	—	0/24/58.50/17.50	7
		1W	12.60	1.5	9.90	0.15	9.90		
		2W	15.60	4	11.00/14.30	0.15	12.70		
		3W	18.50	5.4	10.70/14.50/16.50	0.15	14.50		
	50	0W	—	—	—	—	—	0/28.98/62.35/8.67	8
		1W	12.20	1.5	10.00	0.15	10.00		
		2W	15.70	4	11.00/14.30	0.15	12.70		
		3W	18.20	5.4	10.70/14.50/16.50	0.15	14.50		
	40	0W	—	—	—	—	—	0/37.50/62.50/0	8
		1W	12.20	1.5	10.20	0.15	10.20		
		2W	15.65	4	11.00/14.30	0.15	12.70		
		3W	—	—	—	—	—		
	30	0W	—	—	—	—	—	0/55.50/44.50/0	8
		1W	12.20	1.5	10.40	0.15	10.40		
		2W	14.90	4	11.00/14.50	0.15	12.70		
		3W	—	—	—	—	—		
	20	0W	10.50	—	—	0.15	8.90	31.45/61.80/6.75/0	9
		1W	12.75	1.4	10.00	0.15	10.00		
		2W	14.90	4	11.00/14.00	0.15	12.70		
		3W	—	—	—	—	—		
	10	0W	10.15	—	—	0.15	8.90	45/55/0/0	7
		1W	12.60	1.4	10.00	0.15	10.00		
		2W	—	—	—	—	—		
		3W	—	—	—	—	—		

Table 2: Continued.

	% RH	Layer type	L. Thck	n_{H_2O}	Z_{H_2O}	n_{Ni}	Z_{Ni}	Total contribution 0W/1W/2W/3W	M
Hydration	20	0W	10.15	—	—	0.15	8.90	32/68/0/0	8
		1W	12.30	1.4	10.00	0.15	10.00		
		2W	—	—	—	—	—		
		3W	—	—	—	—	—		
	30	0W	10.50	—	—	0.15	8.90	22.95/63.50/13.55/0	7
		1W	12.40	1.4	10.50	0.15	10.50		
		2W	15.60	3	11.00/14.00	0.15	12.65		
		3W	—	—	—	—	—		
	40 (return)	0W	—	—	—	—	—	0/58.20/41.80/0	6
		1W	12.60	1.5	10.00	0.15	10.00		
		2W	15.20	4	11.00–14.50	0.15	12.80		
		3W	—	—	—	—	—		

Note: layer thickness (L. Thck in Å). n: number of H_2O molecules for hydrated layers (per O_{20} $(OH)_4$). Z: position of H_2O molecule along the c^* axis. n: number of exchangeable cations per half-unit cell. Z: position of exchangeable cations per half-unit cell calculated along c^* axis respectively, for 2W, 1W, and 0W, and M: average layer number per stacking.

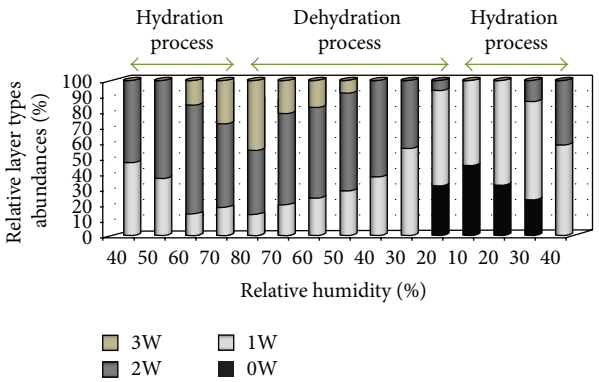

Figure 8: Layer type abundance evolution.

higher RH range (70% up ≤ RH ≤ 70% down), where the best fit of the experimental profiles is achieved using three configurations of MLSs including various proportions of 1W, 2W, and 3W layers types randomly distributed within smectite crystallites (Figure 3). The increase of the hydration heterogeneity is also observed at low humidity range where theoretical models are described, using three layer types characterized by an interstratification, with different contribution, of various hydration states (2W, 1W, and 0W) (Figure 3). All structural parameters and compositions of the used MLS that made it possible to have the best agreement between calculated and experimental XRD patterns throughout the studied cycle are summarized in Table 2.

(2) Sequential Evolution of the Layers Types Contributions. Looking at the layer type abundance evolution (Figure 8), the 3W hydration state appears at 60% RH. This "phases continuum" is reached when increasing RH rate towards high saturated environment (80% RH) with a high proportion (45.36%), which disappears completely along the dehydration process towards 40% RH. For this rate, the structure is modeled by a major contribution of 2W layer (62.50%) and 37.50% of monohydrated layer 1W. The continuous decreasing of RH rate is accompanied by proceeding of the 1W-0W transition where the dehydrated layers types (i.e., 0W) are observed in first time at 20% RH downing accompanied by a decreasing of the relative amount of 2W layers. At low humidity range, the dehydrated layers persist in structure with a significant proportion even with increasing RH% values during the rehydration process to disappear at the end of the cycle (40% RH returning) where the monohydrated layers dominate the interlayer spaces (Figure 8).

3.2. Case of the Dehydration-Hydration Cycle

3.2.1. Qualitative Description of the Dehydration-Hydration Cycle. The full observation of the d_{001} basal spacing progression with the gradual RH values along the reverse cycle shows that two subcycles can be distinguished.

The first one is spread over the low RH field, starting from 40% RH and continuing with lowering RH rate towards extremely dried condition (10% RH), then followed by a hydration process (an increase of the RH rates) to return at 40% RH. Along this path, a slow continuous "2W-1W" transition accompanied by a shift of d_{001} basal spacing value from 15.47 Å to 12.89 Å then increase again to 14.82 Å is observed. The interstratified hydration is the dominated character all over this RH range which is confirmed by the highest FWHM value and the irrational 00ℓ reflection position (Table 1). The second subcycle is founded at the highest RH range beginning from 40% RH (hydration process) to 80% RH and followed by a dehydration process to finish at 40% RH. Throughout this way, a slow evolution of the d_{001} spacing values is observed where the "2W-3W" transition is obtained under RH rates between 60% and 80%. Along the dehydration procedure, the d_{001} basal spacing value shifts from 16.88 Å to 15.20 Å and the same hydration performance law is respected (Figure 7(b)). This behavior can explain the observed hysteresis at this RH field where all calculated FWHM and ξ parameter suggest the interstratified character (Table 1).

Table 3: Structural parameters used to reproduce experimental patterns of SWy-2-Ni as a function of RH along the second cycle.

	% RH	Layer type	L. Thck	n_{H_2O}	Z_{H_2O}	n_{Ni}	Z_{Ni}	Total 0W/1W/2W/3W	M
Dehydration	40 (start)	0W	—	—	—	—	—	0/44/56/0	7
		1W	12.00	1.5	10.80	0.15	10.80		
		2W	15.45	3.6	11.30/14.50	0.15	12.80		
		3W	—	—	—	—	—		
	30	0W	—	—	—	—	—	0/57.5/42.5/0	9
		1W	12.10	1.5	10.60	0.15	10.60		
		2W	15.00	3	11.20/14.20	0.15	12.70		
		3W	—	—	—	—	—		
	20	0W	10.30	—	—	0.15	8.90	17.20/63.05/19.75/0	8
		1W	12.60	1.4	10.40	0.15	10.40		
		2W	14.90	3	11.00/13.80	0.15	12.65		
		3W	—	—	—	—	—		
	10	0W	10.50	—	—	0.15	8.90	36/61/3/0	8
		1W	12.60	1.2	10.20	0.15	10.20		
		2W	15.00	2.8	11.00/14.00	0.15	12.80		
		3W	—	—	—	—	—		
Hydration procedure	20	0W	10.25	—	—	0.15	8.90	20.80/66.60/12.60/0	8
		1W	12.55	1.3	10.50	0.15	10.50		
		2W	14.90	3	10.80/14.00	0.15	12.65		
		3W	—	—	—	—	—		
	30	0W	10.35	—	—	0.15	9.00	13.80/73.35/12.85/0	7
		1W	12.40	1.4	10.30	0.15	10.30		
		2W	14.95	3	10.80/13.80	0.15	12.80		
		3W	—	—	—	—	—		
	40	0W	—	—	—	—	—	0/59.40/40.60/0	8
		1W	12.20	1.5	10.50	0.15	10.50		
		2W	15.40	3.4	11.00/13.70	0.15	12.80		
		3W	—	—	—	—	—		
	50	0W	—	—	—	—	—	0/48/52/0	7
		1W	12.60	1.6	10.60	0.15	10.60		
		2W	15.40	3.6	11.00/13.80	0.15	12.80		
		3W	—	—	—	—	—		
	60	0W	—	—	—	—	—	0/42.75/55.75/1.5	7
		1W	12.70	1.8	10.6	0.15	10.60		
		2W	15.60	3.6	11.00/14.00	0.15	12.40		
		3W	18.00	5.4	10.00/14.40/16.30	0.15	14.40		
	70	0W	—	—	—	—	—	0/29.25/65.75/4.5	7
		1W	12.30	1.8	10.50	0.15	10.50		
		2W	15.80	3.8	11.00/13.80	0.15	12.40		
		3W	18.00	5.4	10.00/14.40/16.30	0.15	14.40		
	80	0W	—	—	—	—	—	0/17/46.2/36.8	8
		1W	12.60	2.5	10.00	0.15	10.00		
		2W	15.80	5	10.90/14.60	0.15	12.70		
		3W	18.90	8.4	10.50/14.90/16.20	0.15	14.90		

Table 3: Continued.

	% RH	Layer type	L. Thck	n_{H_2O}	Z_{H_2O}	n_{Ni}	Z_{Ni}	Total 0W/1W/2W/3W	M
Dehydration	70	0W	—	—	—	—	—	0/27.25/60.95/11.80	8
		1W	12.20	1.8	9.90	0.15	9.90		
		2W	15.85	4	10.90/13.70	0.15	12.40		
		3W	18.60	6.3	10.00/14.50/16.70	0.15	14.50		
	60	0W	—	—	—	—	—	0/34.25/61.25/4.5	8
		1W	12.30	1.8	9.80	0.15	9.80		
		2W	15.80	3.8	11.00/13.70	0.15	12.40		
		3W	18.50	6	10.20/14.70/16.70	0.15	14.70		
	50	0W	—	—	—	—	—	0/42/58/0	8
		1W	12.80	1.6	10.40	0.15	10.40		
		2W	15.60	3.6	11.10/13.80	0.15	12.40		
		3W	—	—	—	—	—		
	40 (return)	0W	—	—	—	—	—	0/55/45/0	9
		1W	12.60	1.6	10.50	0.15	10.50		
		2W	15.80	3.6	11.30–14.20	0.15	12.50		
		3W	—	—	—	—	—		

3.2.2. Quantitative XRD Analysis

(1) Structure Heterogeneity Degree. The simulation of all XRD patterns recorded along the reverse cycle is achieved assuming the coexistence of different MLSs including various relative proportions of layer with different hydration states (Figure 6). Thus the hydration heterogeneity is the main character deduced whatever the relative humidity (RH) values along this second studied cycle. In fact, at 40% RH, two MLSs types with different contribution of 1W and 2W are used to fit experimental patterns. Along dehydration process, the structure becomes more heterogeneous and structural fluctuations continued even with increasing RH% to 30% throughout the hydration process. All experimental XRD patterns recorded along this low relative humidity range are fitted assuming three MLSs structures including different proportion of 0W, 1W, and 2W layers types (Figure 6). The first coming back to 40% RH, is characterized by a decreasing in the MLSs number used for modeling and the disappearing of the dehydrated phases from structure which means a reduction of heterogeneity at this state of the cycle (Figure 6). From 50% up to the higher RH% rates (80% RH) the best agreement is obtained using three MLSs and the hydration heterogeneity increases more with the dehydration process especially at 60% RH and 70% RH downing where the structure is described using four different MLSs indicating the important structural fluctuations at this range of the cycle, whereas the continuous increasing dehydration to return at 40% RH is accompanied by a gradual reorganization in the structure and a notable lowering on MLS is used to fit experimental patterns where just one population is observed at the end of the cycle. Table 3 illustrates the principal structural parameters characterizing the calculated models.

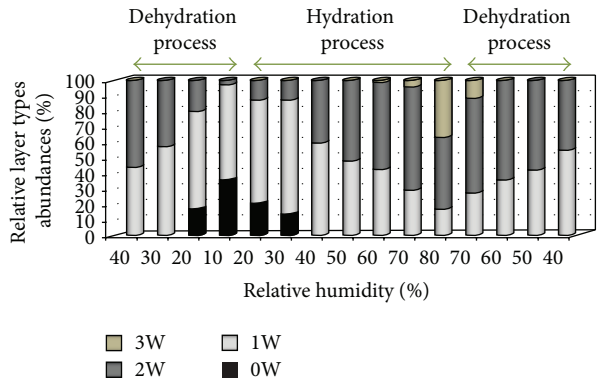

Figure 9: Relative contribution of the different layer types versus the relative humidity values during the reverse cycle.

(2) Sequential Evolution of the Layer Types Contributions. The evolution of the different layer types contribution versus the relative humidity values during the reverse cycle is reported in Figure 9. The dehydration from 40% RH to 10% RH is accompanied by a progressive attenuation on the 2W hydration state contribution and a dominance of 1W layers types in the structure. For the dehydrated phases (i.e., 0W), they appear for the first time at 20% RH downing to reach its peak towards extremely dried condition (10% RH) achieving the height proportion (~36%). These layers types (i.e., 0W) persist within the structure along the hydration procedure

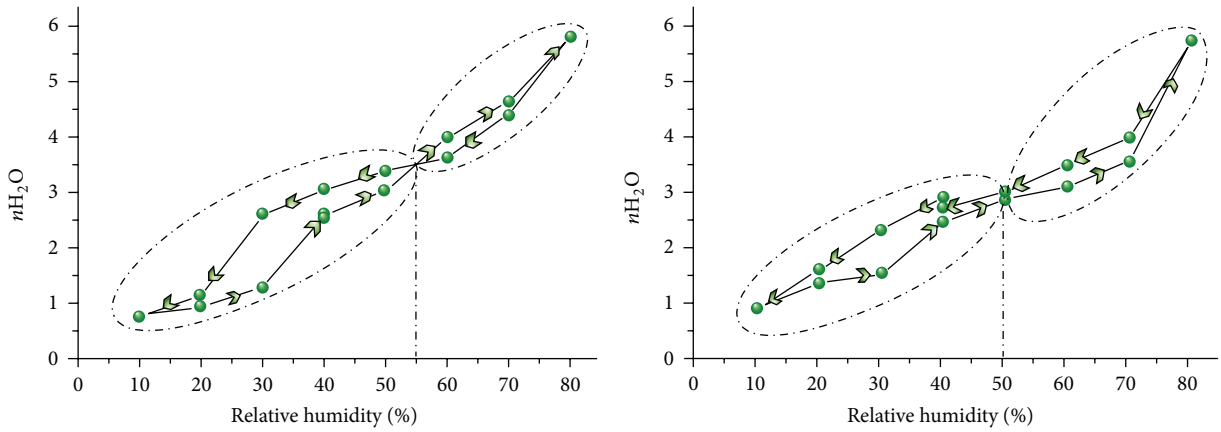

Figure 10: The evolution of the interlamellar water molecule content with the relative humidity, respectively, along the first and the second cycle obtained through the quantitative investigation.

to disappear completely with increasing RH rates towards 40% RH. The continuous increasing of the RH% rates is characterized by a transition from 1W to 2W hydration sates accompanied by the appearance of the 3W phases towards 60% RH, which reach their higher amount (36.80%) at 80% RH. By decreasing towards 40%RH, along the second dehydration process, a continuous 3W → 2W → 1W transition is noted. Indeed, the 3W layer types at 60% RH downing disappeared is observed. Furthermore, the growth of the monohydrated phases (i.e., 1W) amount at the expense of the bihydrated layers types, along this RH range to finish at 40% RH with interlayer's spaces dominated by the 1W phases (55%), is noted.

3.3. Progress of the Interlamellar Water Amounts. The sequential transition from a hydration state to another one that is accruing in interlayer space, at different stages of both cycles, is logically accompanied by a change on the interlayer water amount and distribution. The evolution of the interlamellar water molecule content with the relative humidity, respectively, along the first and the second cycle, obtained through the quantitative investigation is summarized in Figure 10.

3.3.1. Case of the First Cycle. In the case of the first cycle, the global observation of the water content progression showed the appearance of two hystereses where the first is spread at the high humidity field with a small loop, whereas the second stretches in a wide range of humidity between 55% RH and 10% RH (Figure 10(a)). This result can be interpreted as follows.

At the first part of the cycle spreading, over the high humidity range, the effect of the continuous RH rates change has a less influence on the hydration properties and the interlamellar space stability. In this situation, the water molecule distribution is more respected than at the medium and low relative humidity range where several structural fluctuations appear, by the continuous RH rate variation, which induce a perturbation on the interlamellar water molecule amounts evolution. In fact, the decrease of the RH values along the dehydration process, to the extremely dried condition (10% RH), is accompanied by a fast lessening on the water molecule content, which can be explained by a more difficult insertion process of water molecules along the rehydration of the interlayer spaces. Indeed, the water amount distribution is affected and low respected which explains the appearance of the clear hysteresis at this RH% domain.

3.3.2. Case of the Opposite Cycle Orientation. The water amount evolution, along the reverse cycle, is characterized also by the appearance of two hystereses where the first one is extended between 10% and 50% RH range with the biggest loop whereas the second is spread over the higher RH range (Figure 10(b)). Thus we can deduce that the structural fluctuation and the heterogeneity hydration induced by the continuous RH rates variation have significant effects on the water contents especially at the lower RH range, where we showed, at first time, a fast decreasing in the relative water amount during the dehydration process, beginning from the 40% RH to 10% RH, whereas a slow increasing for the interlamellar space water molecule content with continued increasing of the RH values along the rehydration procedure is observed. This behavior suggests that the insertion of the H_2O molecules in the smectite structure becomes more difficult after lowering the RH rate towards extremely dried condition (10% RH) which induce an instability and have a considerable impact on the water content at the higher RH fields where the water amount evolution versus relative humidity displays different trends over these RH range.

The comparison between the water contents retained in the interlayer space at the high RH range of both cycles indicates that the studied sample retains more important water in the case of the first cycle than in the second one. This purpose means that the insertion of H_2O plane in interlayer spaces becomes easier when %RH rates change directly from ambient to high humidity than when the RH values are lowering from the ambient towards the extremely dried RH

condition or to achieve the extremely saturated condition (80% RH). That can suggest that the sequence RH% orientation may act as an intrinsic factor governing the hydration behavior of the studied samples.

4. Conclusion

The XRD profile modeling approach is used in this work to investigate the interlamellar space organization of low-charge montmorillonite under variable relative humidity conditions. All real structure changes are interpreted theoretically using results obtained from calculated XRD models. The main obtained results showed the following.

(1) The Ni-exchanged montmorillonite displays a difference in the hydration behavior as function of the sequence RH orientation.

(2) The interstratified hydration character is the dominated character all over explored RH's range.

(3) The appearance of hysteresis with different loops in the swelling curves indicates the irreversible retained interlayer water amount as function of the relative humidity in both cases of the cycles.

(4) Structural fluctuation, within the smectite structure, is directly dependent on interlamellar water molecule distribution.

Conflict of Interests

The authors declare that there is no conflict of interests regarding the publication of this paper.

Acknowledgments

This project was supported by Deanship of Scientific Research, College of Science Research Center, King Saud University. The results presented are a part of Marwa Ammar's Ph.D. thesis, supervised by Dr. Walid Oueslati. Marwa Ammar acknowledges Walid Oueslati for her main contribution in the XRD modeling approach and the proofreading of the paper. The contribution of Prof. Nejmeddine Chorfi (King Saud University, KSA) in the improvement of the developed code using numerical approach is acknowledged. The content and style of the paper greatly benefited from the comments of two anonymous reviewers.

References

[1] S. S. Gupta and K. G. Bhattacharyya, "Removal of Cd(II) from aqueous solution by kaolinite, montmorillonite and their poly(oxo zirconium) and tetrabutylammonium derivatives," *Journal of Hazardous Materials*, vol. 128, no. 2-3, pp. 247–257, 2006.

[2] Ö. Tunusoğlu, T. Shahwan, and A. E. Eroğlu, "Retention of aqueous Ba^{2+} ions by calcite and aragonite over a wide range of concentrations: characterization of the uptake capacity, and kinetics of sorption and precipitate formation," *Geochemical Journal*, vol. 41, no. 5, pp. 379–389, 2007.

[3] N. Karapinar and R. Donat, "Adsorption behaviour of Cu^{2+} and Cd^{2+} onto natural bentonite," *Desalination*, vol. 249, no. 1, pp. 123–129, 2009.

[4] B. Dou, V. Dupont, W. Pan, and B. Chen, "Removal of aqueous toxic Hg(II) by synthesized TiO_2 nanoparticles and TiO_2/montmorillonite," *Chemical Engineering Journal*, vol. 166, no. 2, pp. 631–638, 2011.

[5] S. H. Lin and R. S. Juang, "Heavy metal removal from water by sorption using surfactant-modified montmorillonite," *Journal of Hazardous Materials*, vol. 92, no. 3, pp. 315–326, 2002.

[6] L.-G. Yan, X.-Q. Shan, B. Wen, and G. Owens, "Adsorption of cadmium onto Al13-pillared acid-activated montmorillonite," *Journal of Hazardous Materials*, vol. 156, no. 1–3, pp. 499–508, 2008.

[7] F. Hubert, L. Caner, A. Meunier, and E. Ferrage, "Unraveling complex <2 μm clay mineralogy from soils using X-ray diffraction profile modeling on particle-size sub-fractions: implications for soil pedogenesis and reactivity," *American Mineralogist*, vol. 97, no. 2-3, pp. 384–398, 2012.

[8] D. Righi and F. Elsass, "Characterization of soil clay minerals: Decomposition of X-ray diffraction diagrams and high-resolution electron microscopy," *Clays and Clay Minerals*, vol. 44, no. 6, pp. 791–800, 1996.

[9] R. W. Mooney, A. G. Keenan, and L. A. Wood, "Adsorption of water vapor by montmorillonite. II. Effect of exchangeable ions and lattice swelling as measured by X-ray diffraction," *Journal of the American Chemical Society*, vol. 74, no. 6, pp. 1371–1374, 1952.

[10] D. M. Moore and R. C. Reynolds, *X-Ray Diffraction and the Identification and Analysis of Clay Minerals*, Oxford University Press, Oxford, UK, 1997.

[11] E. Ferrage, B. Lanson, N. Malikova, A. Plançon, B. A. Sakharov, and V. A. Drits, "New insights on the distribution of interlayer water in bi-hydrated smectite from X-ray diffraction profile modeling of 00*l* reflections," *Chemistry of Materials*, vol. 17, no. 13, pp. 3499–3512, 2005.

[12] E. Ferrage, C. A. Kirk, G. Cressey, and J. Cuadros, "Dehydration of Ca-montmorillonite at the crystal scale. Part 2. Mechanisms and kinetics," *American Mineralogist*, vol. 92, no. 7, pp. 1007–1017, 2007.

[13] W. Oueslati, H. B. Rhaiem, and A. B. H. Amara, "XRD investigations of hydrated homoionic montmorillonite saturated by several heavy metal cations," *Desalination*, vol. 271, no. 1–3, pp. 139–149, 2011.

[14] M. Ammar, W. Oueslati, H. B. Rhaiem, and A. Ben Haj Amara, "Quantitative XRD analysis of the dehydration-hydration performance of (Na^+, Cs^+) exchanged smectite," *Desalination and Water Treatment*, vol. 52, no. 22–24, pp. 4314–4333, 2014.

[15] M. Ammar, W. Oueslati, H. Ben Rhaiem, and A. Ben Haj Amara, "Effect of the hydration sequence orientation on the structural properties of Hg exchanged montmorillonite: quantitative XRD analysis," *Journal of Environmental Chemical Engineering*, vol. 2, no. 3, pp. 1604–1611, 2014.

[16] M. Alshabanat, A. Al-Arrash, and W. Mekhamer, "Polystyrene/montmorillonite nanocomposites: study of the morphology and effects of sonication time on thermal stability," *Journal of Nanomaterials*, vol. 2013, Article ID 650725, 12 pages, 2013.

[17] E. Ferrage, B. Lanson, L. J. Michot, and J.-L. Robert, "Hydration properties and interlayer organization of water and ions in synthetic na-smectite with tetrahedral layer charge. Part 1. Results from X-ray diffraction profile modeling," *The Journal of Physical Chemistry C*, vol. 114, no. 10, pp. 4515–4526, 2010.

[18] E. Ferrage, B. Lanson, B. A. Sakharov, N. Geoffroy, E. Jacquot, and V. A. Drits, "Investigation of dioctahedral smectite hydration properties by modeling of X-ray diffraction profiles: influence of layer charge and charge location," *American Mineralogist*, vol. 92, no. 10, pp. 1731–1743, 2007.

[19] W. Oueslati, M. S. Karmous, H. Ben Rhaiem, B. Lanson, and A. Ben Haj Amara, "Effect of interlayer cation and relative humidity on the hydration properties of a dioctahedral smectite," *Zeitschrift fur Kristallographie*, vol. 2, no. 26, pp. 417–422, 2007.

[20] W. Oueslati, H. Ben Rhaiem, B. Lanson, and A. Ben Haj Amara, "Selectivity of Na-montmorillonite in relation with the concentration of bivalent cation (Cu^{2+}, Ca^{2+}, Ni^{2+}) by quantitative analysis of XRD patterns," *Applied Clay Science*, vol. 43, no. 2, pp. 224–227, 2009.

[21] D. Xu, X. Zhou, and X. Wang, "Adsorption and desorption of Ni^{2+} on Na-montmorillonite: effect of pH, ionic strength, fulvic acid, humic acid and addition sequences," *Applied Clay Science*, vol. 39, no. 3-4, pp. 133–141, 2008.

[22] S. S. Gupta and K. G. Bhattacharyya, "Adsorption of Ni(II) on clays," *Journal of Colloid and Interface Science*, vol. 295, no. 1, pp. 21–32, 2006.

[23] S. S. Gupta and K. G. Bhattacharyya, "Immobilization of Pb(II), Cd(II) and Ni(II) ions on kaolinite and montmorillonite surfaces from aqueous medium," *Journal of Environmental Management*, vol. 87, no. 1, pp. 46–58, 2008.

[24] K. G. Bhattacharyya and S. S. Gupta, "Influence of acid activation on adsorption of Ni(II) and Cu(II) on kaolinite and montmorillonite: kinetic and thermodynamic study," *Chemical Engineering Journal*, vol. 136, no. 1, pp. 1–13, 2008.

[25] X. L. Tan, J. Hu, X. Zhou, S. M. Yu, and X. K. Wang, "Characterization of Lin'an montmorillonite and its application in the removal of Ni^{2+} from aqueous solutions," *Radiochimica Acta*, vol. 96, no. 8, pp. 487–495, 2008.

[26] Z. Liu, J. Yang, Z. Zhang, L. Chen, and Y. Dong, "Study of ^{63}Ni(II) sorption on CMC-bound bentonite from aqueous solutions," *Journal of Radioanalytical and Nuclear Chemistry*, vol. 291, no. 3, pp. 801–809, 2012.

[27] T. Hu and L. Tan, "Sorption/desorption of radionickel on/from Na-montmorillonite: kinetic and thermodynamic studies," *Journal of Radioanalytical and Nuclear Chemistry*, vol. 292, no. 1, pp. 103–112, 2012.

[28] W. F. Moll Jr., "Baseline studies of the clay minerals society source clays: geological origin," *Clays and Clay Minerals*, vol. 49, no. 5, pp. 374–380, 2001.

[29] D. Borden and R. F. Giese, "Baseline studies of the clay minerals society source clays: cation exchange capacity measurements by the ammonia-electrode method," *Clays and Clay Minerals*, vol. 49, no. 5, pp. 444–445, 2001.

[30] A. R. Mermut and A. F. Cano, "Baseline studies of the clay minerals society source clays: chemical analyses of major elements," *Clays and Clay Minerals*, vol. 49, no. 5, pp. 381–386, 2001.

[31] D. Tessier, *Etude expérimentale de l'organisation des matériaux argileux. Hydratation, gonflement et structure au cours de la dessiccation et de la réhumectation [Thèse]*, Université de Paris VII, Publication INRA Versailles, Paris, France, 1984.

[32] J. Srodon, D. J. Morgan, E. V. Eslinger, D. D. Eberl, and M. R. Karlinger, "Chemistry of illite/smectite and end-member illite," *Clays and Clay Minerals*, vol. 34, no. 4, pp. 368–378, 1986.

[33] T. Sato, T. Watanabe, and R. Otsuka, "Effects of layer charge, charge location, and energy change on expansion properties of dioctahedral smectites," *Clays & Clay Minerals*, vol. 40, no. 1, pp. 103–113, 1992.

[34] W. Oueslati, M. Meftah, H. Ben Rhaiem, and A. Ben Haj Amara, "Selectivity of Na-montmorillonite versus concentration of two competitive bivalent cations (Cu^{2+}, Pb^{2+}): quantitative XRD investigation," *Advances in Materials Science and Engineering*, vol. 2009, Article ID 385673, 4 pages, 2009.

[35] E. Ferrage, B. Lanson, B. A. Sakharov, and V. A. Drits, "Investigation of smectite hydration properties by modeling experimental X-ray diffraction patterns: part I: montmorillonite hydration properties," *American Mineralogist*, vol. 90, no. 8-9, pp. 1358–1374, 2005.

[36] T. Watanabe and T. Sato, "Expansion characteristics of montmorillonite and saponite under various relative humidity conditions," *Clay Science*, vol. 7, no. 3, pp. 129–138, 1988.

[37] S. W. Bailey, "Nomenclature for regular interstratifications," *American Mineralogist*, vol. 67, no. 3-4, pp. 394–398, 1982.

[38] J. M. Cases, I. Bérend, M. François, J. P. Uriot, L. J. Michot, and F. Thomas, "Mechanism of adsorption and desorption of water vapor by homoionic montmorillonite: 3. The Mg^{2+}, Ca^{2+}, Sr^{2+} and Ba^{2+} exchanged forms," *Clays and Clay Minerals*, vol. 45, no. 1, pp. 8–22, 1997.

[39] J. Cuadros, "Interlayer cation effects on the hydration state of smectite," *American Journal of Science*, vol. 297, no. 8, pp. 829–841, 1997.

[40] V. A. Drits and B. A. Sakharov, *X-Ray Structure Analysis of Mixed-Layer Minerals*, Nauka, Moscow, Russia, 1976.

[41] V. A. Drits and C. Tchoubar, *X-Ray Diffraction by Disordered Lamellar Structures: Theory and Applications to Microdivided Silicates and Carbons*, Springer, Berlin, Germany, 1990.

[42] B. Lanson, "Modelling of X-ray diffraction profiles: investigation of defective lamellar structure crystal chemistry," in *EMU Notes in Mineralogy*, vol. 11, pp. 151–202, 2011.